J Mater Sci (2011) 46:327–338
DOI 10.1007/s10853-010-4816-6

Toughening of epoxy using core–shell particles

G. Giannakopoulos · K. Masania · A. C. Taylor

Received: 17 June 2010 / Accepted: 3 August 2010 / Published online: 17 August 2010
© Springer Science+Business Media, LLC 2010

Abstract An epoxy resin, cured using an anhydride hardener, has been modified by the addition of preformed core–shell rubber (CSR) particles which were approximately 100 or 300 nm in diameter. The glass transition temperature, T_g, of the cured epoxy polymer was 145 °C. Microscopy showed that the CSR particles were well dispersed through the epoxy matrix. The Young's modulus and tensile strength were reduced, and the glass transition temperature of the epoxy was unchanged by the addition of the CSR particles. The fracture energy increased from 77 J/m^2 for the unmodified epoxy to 840 J/m^2 for the epoxy with 15 wt% of 100-nm diameter CSR particles. The measured fracture energies were compared to those using a similar amount of carboxyl-terminated butadiene-acrylonitrile (CTBN) rubber. The CTBN particles provided a larger toughening effect when compared to CSR particles, but reduced the glass transition temperature of the epoxy. For the CSR-modified epoxies, the toughening mechanisms were identified using scanning electron microscopy of the fracture surfaces. Debonding of the cores of the CSR particles from the shells was observed, accompanied by plastic void growth of the epoxy and shell. The observed mechanisms of shear band yielding and plastic void growth were modelled using the Hsieh et al. approach (J Mater Sci 45:1193–1210). Excellent agreement between the experimental and the predicted fracture energies was found. This analysis showed that the major toughening mechanism, responsible for 80–90% of the increase in fracture energy, was the plastic void growth.

G. Giannakopoulos · K. Masania · A. C. Taylor (✉)
Department of Mechanical Engineering, Imperial College London, South Kensington Campus, London SW7 2AZ, UK
e-mail: a.c.taylor@imperial.ac.uk

Introduction

Epoxy polymers are widely used for the matrices of fibre-reinforced composite materials and as adhesives. When cured, epoxies are amorphous and highly cross-linked (i.e., thermosetting) polymers. This microstructure results in many useful properties for structural engineering applications, such as a high Young's modulus and failure strength, low creep, and good performance at elevated temperatures.

However, the structure of such highly cross-linked thermosetting polymers also leads to a highly undesirable property in that they are relatively brittle materials, with a poor resistance to the initiation and growth of cracks. Nevertheless, it has been well established that the incorporation of a second micro-phase of a dispersed rubber, e.g., [1–5], or a thermoplastic polymer, e.g., [6–8], into epoxy polymers can increase their toughness. Here, the rubber or thermoplastic particles are typically about 1–5 μm in diameter with a volume fraction of about 5–20%. The particles are typically well dispersed, and formed by reaction-induced phase-separation. However, it is difficult to control the particle size, as this is dependent on the curing conditions, and hence, the particle size cannot be systematically varied without changing the matrix properties. The presence of the rubbery or thermoplastic phase typically increases the viscosity of the epoxy resin mixture and reduces the Young's modulus of the cured epoxy polymer.

An alternative route to increase the toughness of epoxies is to use core–shell rubber (CSR) particles. These consist of a soft rubbery core with a hard shell around it. The particles are typically formed by emulsion polymerisation, and then dispersed in the epoxy resin. Hence, it is possible to produce particles with a controlled particle size, unlike with phase-separating rubbers. A range of core and shell

materials may be used, and multilayer particles are often used [9]. The shell is chosen to be compatible with the epoxy matrix, and poly(methylmethacrylate) is often used. Typical core materials include butadiene [10], acrylate polyurethane [11], and siloxane. They have been shown to increase the toughness of both bulk polymers and fibre composites, e.g., [12–15]. Hayes and Seferis [16] have reviewed the use of CSR particles in thermoset polymers and composites; this review also discusses some of the other properties that can be affected by the incorporation of CSR particles.

Rigid, inorganic particles have also been used in the past, as these can increase the toughness without affecting the glass transition temperature of the epoxy. Here, glass beads or ceramic (e.g., silica or alumina) particles with a diameter of between 4 and 100 μm are typically used, e.g., [17–22]. However, these relatively large particles also significantly increase the viscosity of the resin, reducing the ease of processing. In addition, due to the size of these particles they are unsuitable for use with infusion processes for the production of fibre composites as they are strained out by the small gaps between the fibres.

More recently, a new technology has emerged which can increase the mechanical performance of such thermosetting polymers. This is via the addition of a nanophase structure in the polymer, e.g., rigid particles of silica [23–26]. Such nanoparticle-modified epoxies have been shown to not only increase the toughness of the epoxy polymer but also, due to the non-agglomerated nature of the silica particles, not to lead to a significant increase in the viscosity of the epoxy monomer, and were applied as matrices in fibre-composites [27]. However, the toughening increment is small when compared to that of CTBN rubber particles.

The use of CSR particles in this size range may lead to significant increases in the fracture properties of the fibre-composites without altering the processing properties or glass transition temperature of the composite; as would be the case with phase separable rubbers, e.g., carboxyl-terminated butadiene-acrylonitrile (CTBN).

The aims of this study are to investigate the fracture energy of an epoxy polymer modified with three types of CSR particles. The structure/property relationships and the toughening mechanisms will be identified and discussed.

Experimental

Materials

The materials were based upon a one-component hot-cured epoxy formulation. The epoxy resin was a standard diglycidyl ether of bis-phenol A (DGEBA) with an epoxide equivalent weight (EEW) of 185 g/eq., "LY556" (Huntsman, UK). The curing agent was an accelerated methylhexahydrophthalic acid anhydride, "Albidur HE 600" (Nanoresins, Germany).

Three different core–shell rubber (CSR) particles were used, comprising two different particle sizes and three different core materials, namely MX 125, MX 156, and MX 960, see Table 1. The particles consist of a soft rubber core with a harder outer shell, and vary in size and core material [28]. These were supplied as a master batch of the CSR particles pre-dispersed at 25 wt% in DGEBA (Kaneka, Belgium) with an EEW of 220 or 243 g/eq., as shown in Table 1. For comparison, some formulations were prepared using a reactive liquid rubber. This was a carboxyl-terminated butadiene-acrylonitrile (CTBN) rubber, "Hypro CTBN 1300x8" (Emerald Performance Materials, USA), which has a number-average molecular weight of 3,550 g/mol and an acrylonitrile content of 18 wt%. This was used pre-reacted with the DEGBA resin as a 40 wt% CTBN-epoxy adduct, "Albipox 1000" (Nanoresins, Germany).

Different types of bulk epoxy polymer formulations were prepared viz., unmodified epoxy control, epoxy with core–shell rubber, or epoxy with CTBN rubber microparticles. Each CSR particle type was studied as a single-phase-modified epoxy up to a maximum addition of 15 wt% CSR.

Bulk sheets of the unmodified and CSR-modified epoxy materials were prepared. To vary the particle content, the particle-modified resins were mixed with LY556 epoxy to give the correct proportions of particles. The value of the EEW of the blend was calculated and a stoichiometric amount of the curing agent was added. The mixture was stirred, degassed, and poured into moulds which had been coated using "Frekote 550NC" (Henkel, UK) release agent. The plates were cured for 1 h at 90 °C, followed by a post-cure of 2 h at 160 °C.

Table 1 Composition and properties of the CSR particles [28]

Type	Core	Core diameter (nm)	Shell	Diameter (nm)	wt% in master resin	EEW (g/eq.)
MX 125	Styrene-butadiene	100	PMMA	85–115	25	243
MX 156	Poly-butadiene	100	PMMA	85–115	25	243
MX 960	Siloxane	300	PMMA	250–350	25	220

EEW epoxy equivalent weight

Glass transition temperature

The glass transition temperatures of selected cured formulations were measured over a temperature range of 30–180 °C with a scan rate of 10 °C/min using a "Q2000" differential scanning calorimeter (TA Instruments, UK). The value of T_g was taken as the mid-point of the heat flow versus temperature curve and two repeat tests were conducted for each formulation.

Mechanical properties

Tensile dumbbell specimens were machined from bulk plates. These were tested at a displacement rate of 1 mm/min and a test temperature of 21 °C, according to ISO 527 [29, 30]. Five replicate specimens were tested for each formulation. The strain in the gauge length was measured using a clip-on extensometer, and the Young's modulus, E, was calculated as the slope of the stress versus strain curve in the region between 0.4 and 0.8% strain.

The single-edge notch bend (SENB) test was used to determine the fracture energy, G_C, and the fracture toughness, K_C, at the onset of crack growth. Specimens were machined from the bulk plates, and a pre-crack was created by tapping a new razor blade in the root of the notch so that the total crack length, a, was between 0.45 and 0.55 of the specimen width. The best results were achieved when the blade was sufficiently cold, i.e., after being stored in a freezer. The values of K_C and G_C were determined according to ISO 13586 [31], using a displacement rate of 1 mm/min and a test temperature of 21 °C. Six replicate specimens were tested for each formulation. All the specimens failed by unstable crack growth, and hence only single, initiation, values of K_C and G_C were obtained from each specimen.

Microscopy

Atomic force microscopy (AFM) was undertaken to obtain the morphologies using a "MultiMode" scanning probe microscope (Veeco, USA) equipped with a "J" scanner and a "NanoScope IV" controller. A smooth surface was first prepared by cutting samples using a cryo-ultramicrotome, "PowerTome XL" (RMC, UK), at −60 °C. The scans were performed in tapping mode using silicon probes with 5 nm tips. Both height and phase images were recorded at 512 × 512 pixel resolution and a 1 Hz scan speed.

The fracture surfaces of the specimens were examined using scanning electron microscopy (SEM). An Hitachi "S-3400N" microscope was used with an acceleration voltage of 15 kV, and all specimens were coated with a thin layer of sputtered gold before analysis to reduce charging. High-resolution SEM was performed on the fracture surfaces with a field emission gun scanning electron microscope (FEG-SEM). The instrument used was a "Leo 1525" (Carl Zeiss, Germany) equipped with a "Gemini" column. Typically, the accelerating voltage was set at 5 kV. All specimens were coated with an approximately 5-nm thick layer of gold or chromium before imaging to reduce charging.

Results

Microstructure

Microscopy of the unmodified epoxy showed that a homogeneous thermoset polymer was formed, and the microtomed surface of the sample was observed to be flat and devoid of any morphological features, see Fig. 1a. Atomic force microscopy of the 9 wt% CSR-modified formulations showed that the particles were well dispersed in the epoxy, see Fig. 1. The measured diameters of the CSR particles agree well with the values reported in Table 1. The manufacturer's data [28] indicates that the MX 125 and MX 156 particles have the same dimensions, with a core approximately 100 nm in diameter and a mean overall diameter of 85–115 nm. The atomic force microscopy identified the soft cores, which are visible as the dark, circular regions, see Fig. 1b and c for example. The mean diameter of the cores was measured to be 58 ± 19 nm for the MX 125 and 58 ± 13 nm for the MX 156 particles.

The MX 960 CSR particles, the largest particles that were studied, were quoted to be 250–350 nm in diameter. The AFM images, see Fig. 1d, were measured and a mean core diameter of 186 ± 100 nm was obtained. (Note that as the AFM images are of microtomed samples, some variation in the measured core diameter of the CSR particles is due to the particles being sectioned at random deviations from the equator of the particle during the cutting process.)

Figure 1d also shows a ring of lighter colour surrounding the darker soft cores. This would appear to be the PMMA shell of the MX 960 particles, as the phase image indicates that this is slightly harder than the matrix epoxy. The shell was measured as 249 ± 96 nm in outside diameter, and a mean thickness of 63 nm was obtained for the PMMA shell.

For the CTBN-modified epoxy, the rubber phase separated into particles up to 1 μm in diameter. The area fraction of the particles in the matrix was measured to be lower than expected which would indicate that some of some of the CTBN remains in solution in the epoxy rather than phase-separating into particles, see Fig. 1e for example [32].

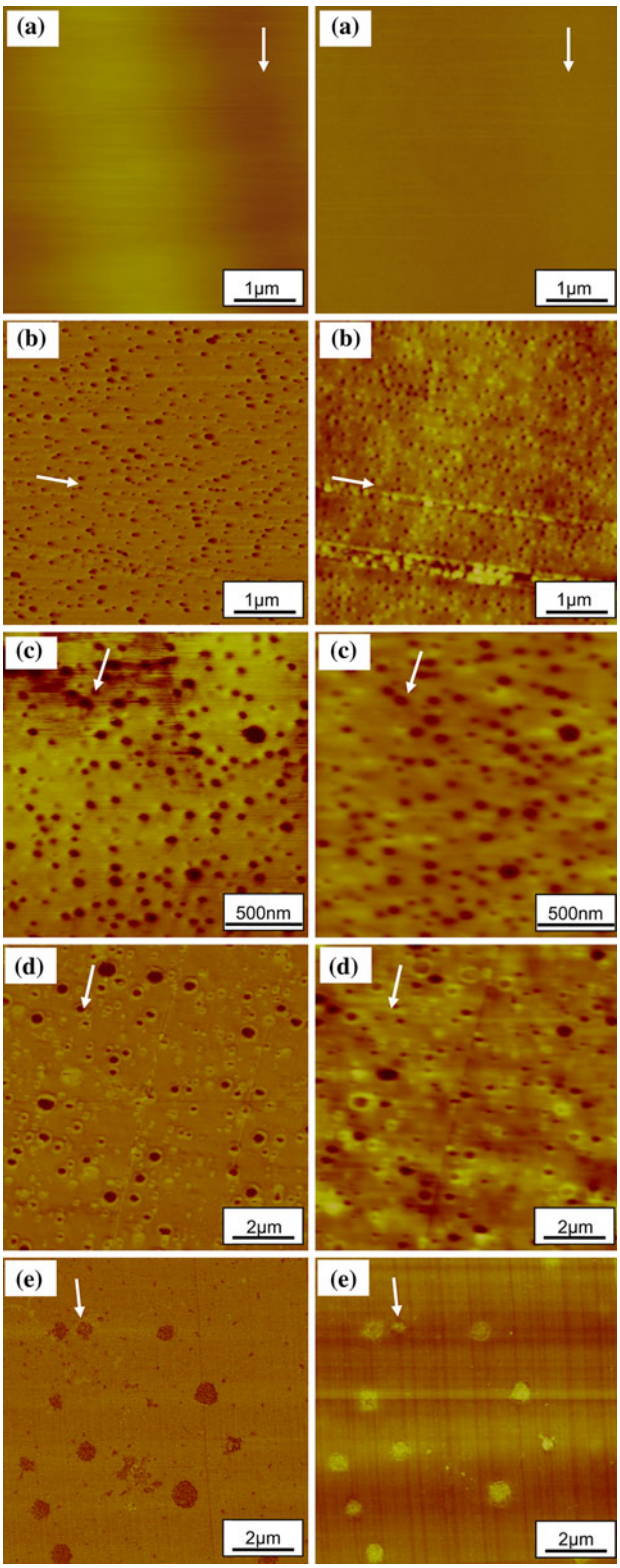

Fig. 1 AFM phase (*left*) and height (*right*) images of the **a** unmodified epoxy, and epoxy modified with **b** 9 wt% MX 125, **c** 9 wt% MX 156, **d** 9 wt% MX 960, and **e** 9 wt% CTBN [32] (the *arrows* indicate the cutting direction)

Glass transition temperature

Differential scanning calorimetry (DSC) was used to determine the glass transition temperature, T_g, of the cured epoxy polymers, as summarised in Table 2. A mean T_g of 145 °C was measured for the unmodified epoxy. Addition of the 9 wt% of CSR did not significantly affect the value of T_g, and values within the range 143–147 °C were measured for epoxies modified with the three CSRs. The T_g of the 9 wt% CTBN-modified epoxy was measured as 137 °C. Based on this decrease in the T_g, and considering the experimental error (±2 °C), Fox's equation [33] was used to deduce that about 1% of the CTBN rubber remains in solution upon curing.

Tensile Young's modulus

A tensile Young's modulus of 2.76 GPa was measured for the unmodified epoxy polymer. The Young's modulus decreased approximately linearly with increasing CSR content, see Fig. 2. The Young's modulus reduced to approximately 2.0 GPa for the 15 wt% CSR-modified epoxies. Generally, the MX 960 CSR-modified epoxies result in slightly lower Young's moduli than the MX 125 or MX 156 counterparts. This may be due to the MX 960 CSR particles possessing a larger volume of the soft core compared to the total particle (core plus shell) volume.

There are various theoretical models that may be used to predict the Young's modulus of a particle-modified polymer, see [34–36] for example. The rule of mixtures, the Halpin–Tsai and the Mori–Tanaka relationships are the most commonly used models. Other models are available, and these are summarised in review papers [37, 38]. All these models make a number of assumptions; they assume that the matrix and the particles are linear-elastic, isotropic and that there is perfect bonding between the particles and the matrix. They also often ignore any agglomeration or particle–particle interactions.

The rule of mixtures and the modified rule of mixtures generally give poor predictions [39], as is the case in this study and these models will not be considered further. The Mori–Tanaka model [40, 41] treats the particles as ellipsoidal (either fibre-like or plate-like) with a constant aspect ratio, and aligned. This model works best for relatively high aspect ratios, but when the aspect ratio approaches unity the model predicts a negligible reinforcing effect. Hence, this model is not suitable for use in this study.

The Halpin–Tsai model, from study by Halpin and co-workers [34, 42], gives the Young's modulus of the material as a function of the Young's modulus of the

Table 2 Glass transition temperature, T_g, Young's modulus, E, and fracture energy, G_C, for the CSR- and CTBN-modified formulations

	wt% CSR	wt% CTBN	T_g (°C)	E (GPa)		G_C (J/m^2)		K_C (MPam$^{1/2}$)	
				Mean	SD	Mean	SD	Mean	SD
Unmodified	0	0	145	2.76	0.08	77	15	0.51	0.02
MX 125	9	0	146	2.32	0.00	596	38	1.16	0.15
MX 156	9	0	143	2.33	0.04	485	41	1.31	0.19
MX 960	9	0	146	2.21	0.02	500	33	1.25	0.16
CTBN [32]	0	9	137	2.35	–	671	50	1.45	0.20

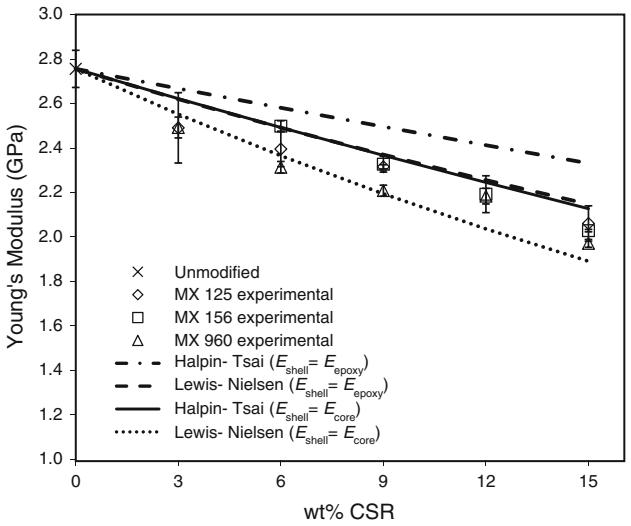

Fig. 2 Young's modulus versus core–shell rubber particle content

matrix polymer, E_m, and of the filler particles, E_f. The predicted composite Young's modulus is

$$E_c = \frac{1 + \zeta\eta v_f}{1 - \eta v_f} E_m \tag{1}$$

where ζ is the shape factor, v_f is the volume fraction of particles, and

$$\eta = \frac{\left(\frac{E_p}{E_u} - 1\right)}{\left(\frac{E_p}{E_u} + \zeta\right)} \tag{2}$$

The inclusion of the shape factor makes the predicted Young's modulus a function of the aspect ratio (w/t) of the particles, where w is the length of the particle and t is its thickness. By comparison of their predictions with the results of a finite-element analysis, Halpin and Kardos [43] suggested that a shape factor of $\zeta = 2w/t$ be used for calculating the Young's modulus of a polymer with the particles aligned with the loading direction. They recommended using $\zeta = 2$ for the Young's modulus perpendicular to the loading direction. CSR particles are spherical, so their aspect ratio is unity, and hence $\zeta = 2$ will be used for this model in this study.

The effect of the level of adhesion between the matrix and the core–shell rubber particles can be considered further using the Lewis–Nielsen model [44] and the study of McGee and McCullough [45]. The composite Young's modulus can be predicted using:

$$E_c = \frac{1 + (k_E - 1)\beta v_f}{1 - \beta\mu v_f} E_m \tag{3}$$

where k_E is the generalised Einstein coefficient, and β and μ are constants. The constant β takes into account the relative Young's modulus of the particles and the matrix, and is given by

$$\beta = \frac{\left(\frac{E_p}{E_u} - 1\right)}{\left(\frac{E_p}{E_u} + (k_E - 1)\right)} \tag{4}$$

The value of μ depends on the maximum volume fraction of particles, v_{max}, and can be calculated from:

$$\mu = 1 + \frac{(1 - v_f)}{v_{max}}[v_{max} v_f + (1 - v_{max})(1 - v_f)] \tag{5}$$

Nielsen and Landel [38] have tabulated values of v_{max} for a range of particle shapes and types of packing. The micrographs indicate that the CSR particles appear non-agglomerated and randomly arranged. For random close packing, non-agglomerated spheres, Nielsen and Landel quote a value of $v_{max} = 0.632$. This value will be used in the Young's modulus predictions.

The value of k_E varies with the degree of matrix to particle adhesion. For a matrix with a Poisson's ratio of 0.5 containing dispersed spheres, $k_E = 2.5$ if there is no slippage at the interface, and $k_E = 1.0$ if there is slippage [38]. Nielsen [46] has shown that the value of k_E is reduced when the Poisson's ratio of the matrix is lower than 0.5. In this study $v = 0.35$ [47], so values of k_E are reduced by a factor of 0.867. Hence, $k_E = 2.167$ if there is no slippage and $k_E = 0.867$ if there is slippage. Here, a value of $k_E = 2.167$ was used giving a good agreement with experimental results.

The densities of the CSR particles were calculated using the density of 1100 kg/m^3 quoted by the manufacturers for the modified resin masterbatch containing 25 wt% of

particles, and an epoxy density of 1180 kg/m^3. This gave a CSR particle density of 910 kg/m^3.

The particles were modelled by assuming a Young's modulus of 3 MPa for the rubbery phase [48]. Although the modulus of the PMMA shell is unknown, lower and upper bounds can be calculated by assuming that its modulus is equal to that of the rubber core or to that of the epoxy, respectively. The predictions are shown with the experimental data in Fig. 2. (Note that the volume fractions of core and shell have been assumed to be equal for the three types of particle used.) The agreement between the predictions and the experimental data is very good, though the lower bound values show the better agreement.

Tensile strength

The tensile strength of the unmodified epoxy was measured to be 83 MPa. It is well known that the addition of particles can reduce the tensile strength of thermoset polymers [12]. The addition of the CSR particles did indeed reduce the tensile strength, and this reduction was approximately linear with increasing particle content, as shown in Fig. 3. For tensile strengths of the materials modified with the MX 125 and MX 156 particles, which are both 85–115 nm in diameter, are approximately equal for each wt% that was studied. Slightly lower tensile strengths were measured for the MX 960 CSR-modified epoxies when compared to the other CSR particles. This may be expected as the MX 960 particles are larger, being approximately three times the diameter of the other CSR particles. The lowest tensile strength was measured to be 53 MPa for the 15 wt% MX 960-modified epoxy.

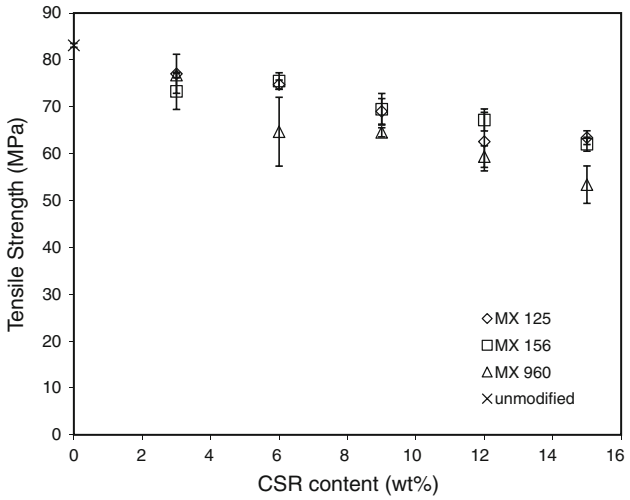

Fig. 3 Tensile strength versus core–shell rubber particle content

Fracture properties

A mean fracture energy, G_C, of 77 J/m^2 was measured for the unmodified epoxy, see Table 2. This value agrees well with that quoted in the literature [32]. The fracture energy was found to increase steadily with the CSR content for the three types of core–shell that were studied, see Fig. 4a–c (the analytical models shown are discussed below). No discernable difference in the fracture energies between the various

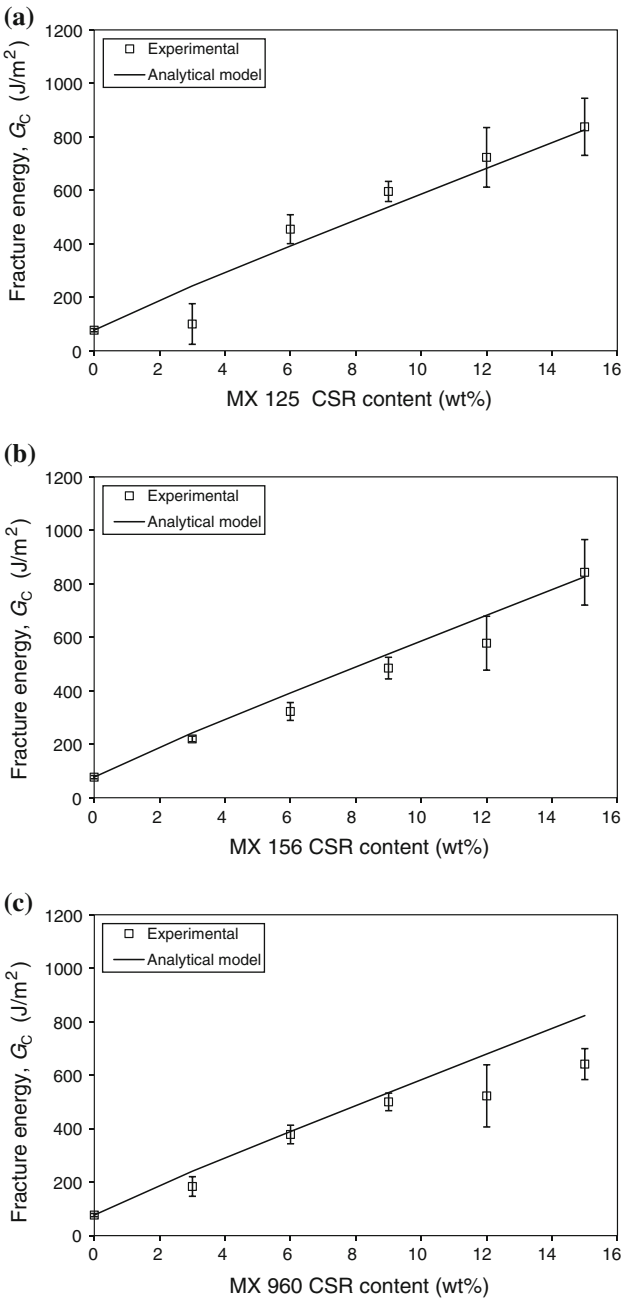

Fig. 4 Fracture energy versus CSR content showing experimental data (*points*) compared to the predictive model (*solid line*) for **a** the MX 125, **b** MX 156, and **c** MX 960 CSR-modified epoxies

particle modifications was obtained when the standard deviation of the mean is considered. The general trend in the mean values suggests that the MX 125 particles show a slightly greater toughening effect than the other CSR particles. A maximum fracture energy of about 840 J/m^2 was measured, using the 15 wt% of MX 125 and MX 156 particles. The maximum fracture energy for the MX 960-modified epoxy was 642 J/m^2, using the 15 wt% of CSR.

The fracture toughness, K_C, of the epoxy also increased with the addition of CSR particles from 0.51 MPam$^{1/2}$ for the unmodified resin to approximately 1.45 MPam$^{1/2}$ for the formulations containing the 15 wt% MX 125 or MX 156, and 1.30 MPam$^{1/2}$ in the case of the 15 wt% MX 960 CSR-modified formulation.

The measured increase in the fracture energy due to the addition of the CSR particles can be compared to that using an equal weight content of CTBN. Hsieh et al. [32] report a fracture energy of 671 J/m^2 for the 9R anhydride cured DGEBA epoxy. This compares with values of between 485 and 600 J/m^2 for the CSR particles used in this study. Similarly, a fracture toughness of 1.45 MPam$^{1/2}$ was measured for the 9R formulations, which compares with values in the range 1.16–1.31 MPam$^{1/2}$ for the 9 wt% CSR-modified systems used in this study, see Table 2.

It must be considered that the comparisons between CTBN and CSR have been made for equal additions of modifier to the epoxy. Due to the PMMA shell, the CSR particles contain less rubber than the CTBN particles. If the data are compared on an equal volume of rubber basis, then the 9 wt% of CTBN is approximately equivalent to 14 wt% of CSR particles. Examination of Table 4 shows that the fracture energy of the CSR-modified epoxies would be very similar to that of the CTBN-modified epoxy at this content.

Fractography

The fracture surfaces of the unmodified epoxy polymer were found to be smooth and glassy. This suggests that no large-scale plastic deformation occurred during fracture, which is typical of a brittle thermosetting polymer [32], and hence a low fracture energy of 77 J/m^2 was measured. Feather markings, caused by the crack forking due to the excess of energy associated with the relatively fast crack growth, are present on the fracture surfaces. This repeated forking and the multi-planar nature of the surface are ways of absorbing this excess energy in a very brittle material [49].

The fracture surfaces of the CSR particle-modified materials showed evidence of crack forking and feather markings, and the fracture surfaces have a relatively brittle appearance. However, the surfaces are rougher than those of the unmodified epoxy, and additional features were observed.

An electron micrograph of the 9 wt% MX 960-modified epoxy, which uses the largest diameter of the CSR particles used in this study, is shown in Fig. 5a. The fracture surfaces were covered with broken CSR particles, typically consisting of bright rubber cores sitting within the dark rings of plastic voids in the epoxy. The particle diameters were measured from the FEG–SEM images and slightly larger mean values of the core diameter were obtained when compared to the measurements from AFM images, as discussed previously. The mean diameter of the cores was measured from images of fracture surfaces (215 nm) and was found to be 1.16 times that from AFM. This would also suggest that the CSR was stretched during the void growth process. The mean diameter of the dark rings was measured to be 269 nm, which is 1.45 times the mean core diameter as measured from AFM (186 nm). Hence, an

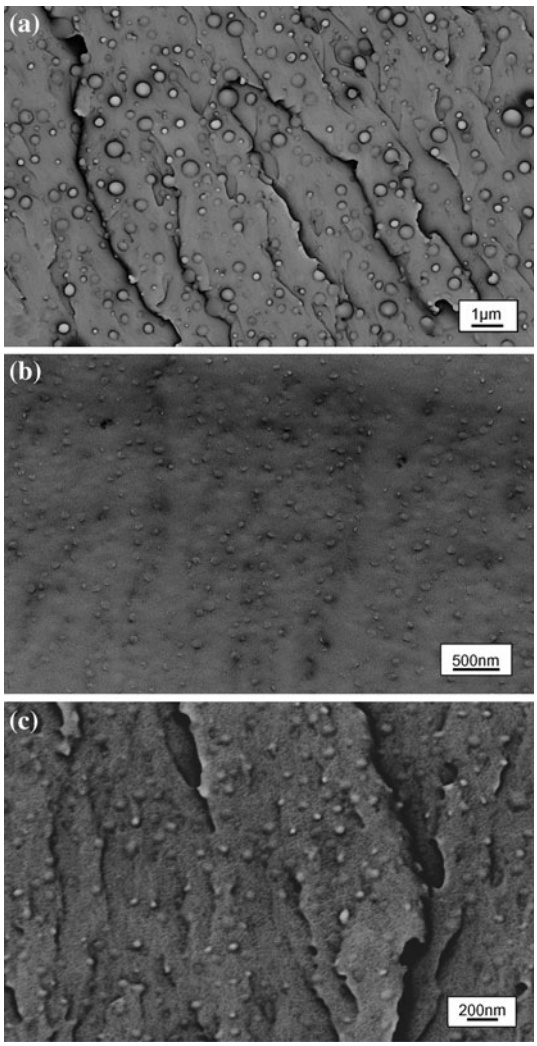

Fig. 5 FEG–SEM images of fracture surface of epoxy with 9 wt% of **a** MX 960 **b** MX 125, and **c** MX 156 CSR particles

initial stretching and debonding process of the cores was followed by plastic void growth of the epoxy polymer, caused by the stress triaxiality just ahead of the crack tip.

For the MX 125 and the MX 156 CSR-containing epoxies, the particles were more difficult to observe due to their smaller diameters of about 100 nm. Figure 5b shows a typical fracture surface for the 9 wt% MX 125 epoxy with evidence of debonded cores in the CSR particles and plastic void growth in the epoxy. Figure 5c shows that similar features were observed on the fracture surfaces of the 9 wt% MX 156 epoxy. Evidence of debonded cores was readily observed on the fracture surfaces and the core diameters were measured to be 47 ± 11 nm, i.e., a similar size as that from the AFM-measured core diameters of 58 ± 13 nm. The rings were measured to have a mean outer diameter of 66 ± 14 nm. Plastic void growth in the epoxy was evident in the epoxy matrix for both the MX 125 and the MX 156 CSR formulations.

The fracture surface of the CTBN-modified epoxy polymer was shown by Hsieh et al. [32] to possess voids, 1.24 μm in diameter. These were formed by the cavitation of the rubber particles followed by plastic void growth of the epoxy.

Toughening micromechanisms

Atomic force microscopy of the CSR particle-modified epoxies showed that the CSR particles were well dispersed through the epoxy polymer. The fracture surfaces of these materials showed many broken CSR particles. These are visible either as depressions, or as the light cores with dark rings around them. These features show that the cores debond prior to fracture. There was no evidence of internal cavitation of the CSR particles occurring, as shown by the rubber cores remaining in the voids that were formed. Shear band yielding has previously been reported for this epoxy in [32], and will be expected to occur. Hence, plastic void growth of the epoxy polymer and shear yielding are the toughening mechanisms for these CSR particle-modified epoxies.

For core–shell particles, previous authors have observed shear yielding and cavitation of the particles. Sue [50, 51] used transmission electron microscopy to show extensive particle cavitation around a sub-critically loaded crack tip, with plastic void growth followed by the formation of shear bands. Pearson and Yee [12] reported particle cavitation and shear banding toughening mechanisms in epoxy with methacrylated butadiene-styrene CSR particles. Either particle cavitation or debonding will create voids, relieving the triaxial stress state ahead of the crack-tip, and allowing plastic void growth. Cavitation and debonding are competitive processes, as cavitation will occur when the rubber is strongly bonded to the surrounding polymer and debonding will occur when the bonding is weak. Based on FEG–SEM observations of the fracture surface, the core to shell adhesion seemed to be relatively low for the CSR particles in this study.

The toughening mechanisms caused by the addition of CTBN to epoxy have been well described previously [5, 47, 52]. The CTBN was present as dispersed rubber microparticles with a mean diameter of approximately 0.54 μm. Scanning electron microscopy of the fracture surfaces showed that these particles cavitate, and that this cavitation process is followed by plastic hole growth of the epoxy polymer. The mean diameter of the cavitated rubber particles was measured to be 1.24 ± 0.46 μm, showing that significant plastic deformation of the epoxy has occurred. Hence, the rubber particles greatly increase the toughness of the material, see Table 2, via interactions of the stress field ahead of the crack tip and the rubber particles, which leads to this greatly enhanced plastic deformation of the epoxy polymer [53–55]. The cavitation process has been modelled, most recently by Guild et al. [56] who developed a criterion to predict whether cavitation would occur and showed that smaller rubber particles require higher strains for cavitation to occur.

Modelling studies

As discussed above, toughening occurred via shell debonding from the core, and subsequent plastic void growth and shear band yielding. The mechanisms of shear band yielding and plastic void growth were modelled by Hsieh et al. [32], who modified the Huang and Kinloch [57] model. Although this model was originally developed for CTBN-modified epoxy [57], and more recently for epoxy modified with silica nanoparticles [32], these predictive models are pertinent to the toughening mechanisms that occurred in the CSR-modified epoxies in this study.

Huang and Kinloch [57] proposed a generalised solution to examine the incremental increase in G_C as

$$G_C = G_{CU} + \Psi \tag{6}$$

where G_{CU} is the fracture energy of the unmodified epoxy polymer and Ψ represents the overall toughening contribution provided by the presence of the particulate phase. The toughening increment due to the CSR particles is a combination of two mechanisms identified from the experimental work. This can be separated into the relative toughening contributions, of (i) plastic shear band yielding, ΔG_s, and (ii) plastic void growth of the epoxy polymer, ΔG_v.

$$\Psi = \Delta G_s + \Delta G_v \tag{7}$$

The energy contribution from plastic shear band yielding, ΔG_s, initiated by the presence of the CSR particles is related to the size of the plastic zone from [32] as

$$\Delta G_s = 0.5 v_f \sigma_{yc} \gamma_f F'(r_y) \tag{8}$$

where v_f is the volume fraction of CSR particles, σ_{yc} is the plane strain compressive true yield stress, and γ_f, the true fracture strain for the unmodified epoxy. The $F'(r_y)$ term takes a modified form of the original formulation of the model [57], and is given by

$$F'(r_y) = r_y \left[\left(\frac{4\pi}{3v_f} \right)^{1/3} \left(1 - \frac{r_p}{r_y} \right)^3 - \frac{8}{5} \left(1 - \frac{r_p}{r_y} \right) \left(\frac{r_p}{r_y} \right)^{5/2} - \frac{16}{35} \left(\frac{r_p}{r_y} \right)^{7/2} - 2 \left(1 - \frac{r_p}{r_y} \right)^2 + \frac{16}{35} \right] \tag{9}$$

The value of r_y is defined as

$$r_y = K_p^2 \left(1 + \frac{\mu_m}{3^{1/2}} \right)^2 r_{pz} \tag{10}$$

where r_p is the particle radius, K_p is the maximum stress concentration for the von Mises stresses around a rigid particle, μ_m is a material constant which allows for the pressure-dependency of the yield stress. The value of μ_m was shown by Sultan and McGarry [58] to be in the range from 0.175 to 0.225 (taken as 0.2). The value of K_p is dependent on the volume fraction of particles, and was calculated by linear regression of the data from Guild and Young [59]. (Note that K_p was quoted by Guild and Young for glass particles in an epoxy matrix, and the values are taken as a first approximation although core–shell particles were used in this study.) The value of K_p varies from approximately 1.65 to 1.74 for the range of volume fractions used in this study.

The value of r_{pz}, the Irwin prediction of plane strain plastic zone radius for the unmodified epoxy at fracture, was calculated from [60] as

$$r_{pz} = \frac{1}{6\pi} \frac{K_{CU}^2}{\sigma_{yt}^2} \tag{11}$$

where K_{CU} is the fracture toughness and σ_{yt} is the tensile true yield strength for the unmodified epoxy polymer.

The contribution of ΔG_v via the plastic void growth mechanism was taken from [57] as

$$\Delta G_v = \left(1 - \frac{\mu_m^2}{3} \right) (v_{fv} - v_f) \sigma_{yc} r_{pz} K_v^2 \tag{12}$$

where μ_m is a material constant (as above), v_{fv} and v_f are the volume fraction of voids and the volume fraction of CSR particles which debond, respectively. The value of v_{fv} was calculated from a void radius of $(1 + \gamma_f) r_p$ [32], i.e., the maximum hoop strain that a shell void could form. The calculated value of v_{fv} agrees well with the values measured from the fracture surfaces, within experimental error, bearing in mind the variation in core diameter and that the crack will not have passed through the equator of most of the voids. All the particles on the fracture surface appeared to debond. K_v is taken as the von Mises stress concentration factor for voids from Guild and Young [61]. The value of K_v varies linearly between 2.11 and 2.12 for the volume fractions considered in this study.

A generalised expression for Ψ may be evaluated by combining Eqs. 8 and 12 into 7 to give

$$\Psi = 0.5 v_f \sigma_{yc} \gamma_f F'(r_y) + \left(1 - \left(\frac{\mu_m^2}{3} \right) \right) (v_{fv} - v_f) \sigma_{yc} r_{pz} K_v^2 \tag{13}$$

The experimental values that were used for the modelling are summarised in Table 3. All the particles on the fracture surface appeared to debond, hence, all the particles in the process zone were taken to initiate shear bands and also debond with plastic void growth of the epoxy.

Calculations were performed for the three types of core–shell particles, and the results are summarised in Table 4, although, those for the MX 125 and the MX 156 epoxies are identical because the particles are the same diameter.

Table 3 Parameters and values for the modelling studies to predict the fracture energy

Name	Variable	Value	Source
Radius of the core–shell particles	r_p (nm)	50 or 150	This study
Radius of the core–shell voids	r_{pv} (nm)	$(1 + \gamma_f) r_p$	[32]
Poisson's ratio	v	0.35	[47]
Plane strain compressive yield true stress	σ_{yc} (MPa)	120	[32]
Plane strain compressive fracture true strain	γ_f	0.75	[32]
Uniaxial tensile yield true stress	σ_{yt} (MPa)	88	[32]
Pressure-dependent yield stress parameter	μ_m	0.2	[58]
Fracture energy	G_{CU} (J/m^2)	77	This study
Fracture toughness	K_{CU} (MPam$^{1/2}$)	0.51	This study

Note: all mechanical properties are for the unmodified epoxy polymer

Table 4 Predicted and measured fracture energies of the (a) MX 125, (b) MX 156, and (c) MX 960 CSR-modified epoxies

(a) MX 125 content		ΔG_s (J/m^2)	ΔG_v (J/m^2)	G_C predicted (J/m^2)	G_C experimental (J/m^2)	
wt%	v_f				Mean	SD
0	0.00	0	0	77	77	15
3	0.03	31	135	243	100	78
6	0.07	44	270	392	455	54
9	0.10	54	407	538	596	38
12	0.13	62	544	682	723	111
15	0.16	68	682	826	838	107
(b) MX 156 content		ΔG_s (J/m^2)	ΔG_v (J/m^2)	G_C predicted (J/m^2)	G_C experimental (J/m^2)	
wt%	v_f				Mean	SD
0	0.00	0	0	77	77	15
3	0.03	31	135	243	220	11
6	0.07	44	270	392	323	33
9	0.10	54	407	538	485	41
12	0.13	62	544	682	578	101
15	0.16	68	682	826	843	122
(c) MX 960 CSR content		ΔG_s (J/m^2)	ΔG_v (J/m^2)	G_C predicted (J/m^2)	G_C experimental (J/m^2)	
wt%	v_f				Mean	SD
0	0.00	0	0	77	77	15
3	0.03	29	135	241	184	37
6	0.07	42	270	389	378	35
9	0.10	51	407	535	500	33
12	0.13	58	544	679	523	115
15	0.16	64	682	823	642	58

It is of note, that the shear banding term is particle size-dependant, i.e., smaller particles provide a greater contribution to the value of ΔG_s. However, the individual contribution of ΔG_v far exceeds that of ΔG_s to the overall fracture energy of the epoxy polymer, indicating that for this system between 80 and 90% of the toughening is due to plastic void growth. Note that the contribution of plastic void growth mechanisms to the fracture energy, ΔG_v, is independent of particle size. Hsieh et al. [32] used the same epoxy, but modified with silica nanoparticles. They reported that the contributions of shear yielding and plastic void growth were approximately equal, because only 15% of the silica nanoparticles debonded.

The predictive model agrees very well with the experimental data, as shown in Fig. 4. An improvement of about 550% was obtained for the 9 wt% MX 960 CSR-modified epoxy with $G_C = 500$ J/m^2, but does not toughen as efficiently as phase separating rubbers, with $G_C = 671$ J/m^2 for the 9 wt% CTBN-modified epoxy, see Table 2, due to the presence of the PMMA shell which reduces the effective volume fraction of rubber. When equal volume fractions of rubber were compared, then the toughening effects are approximately equal. However, CSR particles do toughen without the reductions in T_g and E that are incurred when working with phase separable rubbers.

Based on toughening by shear band yielding and plastic void growth mechanisms, the model predicts that these formulations fulfil the limit of toughening for these two mechanisms using this epoxy. Because the contribution of the plastic void growth mechanism is so dominant, little variation in the fracture energy with particle size is predicted.

Conclusions

An epoxy resin cured with an anhydride was modified by the addition of core–shell rubber (CSR) particles. These particles were well dispersed through the epoxy matrix, with no agglomeration being observed using atomic force microscopy. The glass transition temperature of the epoxy was 145 °C. The addition of CSR particles did not alter the measured value of T_g, but the Young's modulus of the epoxy was reduced. The measured Young's moduli were compared to theoretical values, calculated using the Halpin–Tsai and Lewis–Nielsen models, and good agreement was found.

A fracture energy of 77 J/m^2 was measured for the unmodified epoxy polymer. Addition of the CSR particles increased the fracture energy, a maximum value of 840 J/m^2 was measured for the epoxy with the 15 wt% of 115-nm diameter MX 125 CSR particles. Scanning electron microscopy of the fracture surfaces showed that core to shell debonding followed by plastic void growth of the epoxy, plus shear yielding, were the toughening mechanisms. The measured fracture energies were compared to those using a similar amount, 9 wt%, of a carboxyl-terminated butadiene-acrylonitrile (CTBN) rubber. The CTBN particles gave a greater fracture energy than using the CSR particles, with a G_C of 671 J/m^2 being measured compared to fracture energies of 480–600 J/m^2 for the CSR formulations. However, for equal volume fractions of rubber the fracture energies for the CSR- and CTBN-modified epoxies are very similar.

The operative toughening mechanisms of (i) shear band yielding and (ii) core to shell debonding and plastic void growth were modelled. Excellent agreement was seen between the experimental and the predicted fracture energies. No effect of particle size on the predicted fracture energy was identified for the 100 and the 300-nm diameter particles employed.

Acknowledgements The authors would like to thank Kaneka (D. Sober) and Nanoresins (S. Sprenger) for the supply of materials. They also acknowledge the EPSRC for a doctoral training award for K. Masania, and Becker Industrial Coatings for supporting G. Giannakopoulos. Some of the equipment used was provided by A.C. Taylor's Royal Society Mercer Junior Award for Innovation.

References

1. Drake RS, Siebert AR (1975) SAMPE Q 6:11
2. Kinloch AJ, Shaw SJ, Tod DA, Hunston DL (1983) Polymer 24:1341. doi:10.1016/0032-3861(83)90070-8
3. Kinloch AJ (2003) MRS Bull 28:445
4. Rowe EH, Siebert AR, Drake RS (1970) Mod Plast 47:110
5. Pearson RA, Yee AF (1986) J Mater Sci 21:2475. doi:10.1007/BF01114294
6. Pascault JP, Williams RJJ (1999) In: Paul DR, Bucknall CB (eds) Polymer blends, volume 1: formulation. Wiley, New York
7. Bucknall CB, Partridge IK (1983) Polymer 24:639. doi:10.1016/0032-3861(83)90120-9
8. Kinloch AJ, Yuen ML, Jenkins SD (1994) J Mater Sci 29:3781. doi:10.1007/BF00357349
9. Day RJ, Lovell PA, Pierre D (1997) Polym Int 44:288
10. Qian JY, Pearson RA, Dimonie VL, Elaasser MS (1995) J Appl Polym Sci 58:439
11. Shen J, Zhang Y, Qiu J, Kuang J (2004) J Mater Sci 39:6383. doi:10.1023/B:JMSC.0000043763.65417.4f
12. Pearson RA, Yee AF (1991) J Mater Sci 26:3828. doi:10.1007/BF01184979
13. Lin K-F, Shieh Y-D (1998) J Appl Polym Sci 70:2313
14. Becu-Longuet L, Bonnet A, Pichot C, Sautereau H, Maazouz A (1999) J Appl Polym Sci 72:849
15. Day RJ, Lovell PA, Wazzan AA (2001) Compos Sci Technol 61:41
16. Hayes BS, Seferis JC (2001) Polym Compos 22:451
17. Young RJ, Beaumont PWR (1975) J Mater Sci 10:1343. doi:10.1007/BF00540824
18. Spanoudakis J, Young RJ (1984) J Mater Sci 19:473. doi:10.1007/BF00553571
19. Amdouni N, Sautereau H, Gerard JF (1992) J Appl Polym Sci 46:1723
20. Lee J, Yee AF (2000) Polymer 41:8363
21. Kawaguchi T, Pearson RA (2003) Polymer 44:4239
22. Kitey R, Tippur HV (2005) Acta Mater 53:1167
23. Kinloch AJ, Lee JH, Taylor AC, Sprenger S, Eger C, Egan D (2003) J Adhes 79:867
24. Kinloch AJ, Mohammed RD, Taylor AC, Eger C, Sprenger S, Egan D (2005) J Mater Sci 40:5083. doi:10.1007/s10853-005-1716-2
25. Ragosta G, Abbate M, Musto P, Scarinzi G, Mascia L (2005) Polymer 46:10506
26. Zhang H, Zhang Z, Friedrich K, Eger C (2006) Acta Mater 54:1833
27. Kinloch AJ, Masania K, Taylor AC, Sprenger S, Egan D (2008) J Mater Sci 43:1151. doi:10.1007/s10853-007-2390-3
28. Sober DJ (2008) Personal Communication. Kaneka, Houston
29. ISO-527–1 (1993) Plastics—determination of tensile properties—part 1: general principles. ISO, Geneva
30. ISO-527–2 (1996) Plastics—determination of tensile properties—part 2: test conditions for moulding and extrusion plastics. ISO, Geneva
31. ISO-13586 (2000) Plastics—determination of fracture toughness (G_{IC} and K_{IC})—linear elastic fracture mechanics (LEFM) approach. ISO, Geneva
32. Hsieh T-H, Kinloch AJ, Masania K, Sohn Lee J, Taylor AC, Sprenger S (2010) J Mater Sci 45:1193. doi:10.1007/s10853-009-4064-9
33. Fox TG (1956) Bull Am Phys Soc 1:123
34. Halpin JC, Pagano NJ (1969) J Compos Mater 3:720
35. Kerner EH (1956) Proc Phys Soc B 69:808
36. Nielsen LE (1966) J Appl Polym Sci 10:97
37. Ahmed S, Jones FR (1990) J Mater Sci 25:4933. doi:10.1007/BF00580110
38. Nielsen LE, Landel RF (1994) Mechanical properties of polymers and composites. Marcel Dekker, New York
39. Kinloch AJ, Taylor AC (2006) J Mater Sci 41:3271. doi:10.1007/s10853-005-5472-0
40. Fornes TD, Paul DR (2003) Polymer 44:4993
41. Luo J-J, Daniel IM (2003) Compos Sci Technol 63:1607
42. Halpin JC (1969) J Compos Mater 3:732
43. Halpin JC, Kardos JL (1976) Polym Eng Sci 16:344
44. Lewis TB, Nielsen LE (1970) J Appl Polym Sci 14:1449
45. McGee S, McCullough RL (1981) Polym Compos 2:149
46. Nielsen LE (1968) J Compos Mater 2:120
47. Kinloch AJ (1987) Adhesion and adhesives: science and technology. Chapman & Hall, London
48. Kunz SC, Beaumont PWR (1981) J Mater Sci 16:3141. doi:10.1007/BF00540323
49. Andrews EH (1968) Fracture in polymers. Oliver & Boyd, Edinburgh
50. Sue H-J (1991) Polym Eng Sci 31:275
51. Sue H-J (1991) Polym Eng Sci 31:270
52. Karger-Kocsis J, Friedrich K (1992) Colloid Polym Sci 270:549
53. Cheng C, Hiltner A, Baer E, Soskey PR, Mylonakis SG (1995) J Mater Sci 30:587. doi:10.1007/BF00356315
54. Azimi HR, Pearson RA, Hertzberg RW (1996) Polym Eng Sci 36:2352
55. Chen TK, Jan YH (1992) J Mater Sci 27:111. doi:10.1007/BF02403652
56. Guild FJ, Kinloch AJ, Taylor AC (2010) J Mater Sci 45:3882. doi:10.1007/s10853-010-4447-y

57. Huang Y, Kinloch AJ (1992) J Mater Sci 27:2763. doi:10.1007/BF00540703
58. Sultan JN, McGarry FJ (1973) Polym Eng Sci 13:29
59. Guild FJ, Young RJ (1989) J Mater Sci 24:298. doi:10.1007/BF00660971
60. Caddell RM (1980) Deformation and fracture of solids. Prentice-Hall, Englewood Ciffs
61. Guild FJ, Young RJ (1989) J Mater Sci 24:2454. doi:10.1007/BF01174511